Geochimica et Cosmochimica Acta 376 (2024) 25–36

Contents lists available at ScienceDirect

Geochimica et Cosmochimica Acta

journal homepage: www.elsevier.com/locate/gca

Characterizing sulfur redox state and geochemical implications in deep-time using mineral chemistry network analysis

Eli K. Moore [a,*], Joseph E. Diedolf IV [b], Shaunna M. Morrison [c], Daniel R. Hummer [d]

[a] U.S. Geological Survey, Geology, Energy & Minerals Science Center, Reston, VA 20192, United States
[b] Department of Environmental Science, School of Earth and the Environment, Rowan University, Glassboro, NJ, United States
[c] Earth and Planets Laboratory, Carnegie Institution for Science, Washington, DC, United States
[d] School of Earth Systems and Sustainability, Southern Illinois University, Carbondale, Il, United States

ARTICLE INFO

Associate editor: Nicholas Tosca

Keywords:
Sulfur
Redox
Mineral
Network
Deep-time

ABSTRACT

Sulfur (S) is a central element in global biogeochemical cycling and Earth's redox evolution. Minerals that contain S are an important record of local environmental conditions at the time of their formation based on chemical speciation and redox. However, the oxidation state of S for hundreds of different S-containing minerals and thousands of S-containing mineral localities is unknown, largely sulfides and sulfosalts, and the redox state alone does not fully capture mineral chemistry diversity, thus limiting understanding of S redox evolution. Here, we use mineral chemistry network analysis and the weighted Mineral Element Electronegativity Coefficient of Variation ($wMEE_{CV}$) metric to investigate the element interactions and localities of S-containing minerals from the Mineral Evolution Database (MED) to infer the redox state of S in minerals where the redox state is unknown (S^U). Louvain community detection of the S mineral chemistry redox network reveals that there are three main network communities that are separated by redox state. The S^{6+} community includes minerals that contain the S^{6+} redox state and a small number of S^{4+} and S^{2+} minerals, the S^{2-} community includes S^{2-}-containing minerals, and the S^U community includes minerals in which the redox state of S is unknown. The $wMEE_{CV}$ values of the S^U community closely overlap with the $wMEE_{CV}$ values of the S^{2-} community, and do not overlap with the $wMEE_{CV}$ values of the S^{6+} community, indicating the S^U community minerals contain predominately reduced S. Assuming that S^U community minerals contain reduced S, as supported by their network chemical associations and $wMEE_{CV}$ values, then reduced S-containing minerals make up approximately 81 % of S-containing mineral localities in the S mineral chemistry network, even though the majority of all mineral localities (S-containing and non-S-containing) are oxygen (O)-containing minerals. Additionally, reduced S-containing minerals make up the majority (~75 %) of all non-O containing mineral localities in the MED, representing the importance of reduced S as an electron source and substrate in the evolution of microbial metabolic networks. The range $wMEE_{CV}$ values of S^{6+} community minerals expands through time due primarily to formation of chemically diverse sulfate minerals, coinciding with crustal oxidation from the late Proterozoic to Phanerozoic and the expansion of the marine sulfate reservoir. The intersection of shared constituent elements among reduced and oxidized S in the mineral chemistry network represents redox convergence of weathered S in the geosphere that was crucial in the formation of natural resource deposits and the evolution of biogeochemical cycles.

1. Introduction

1.1. Geochemistry of sulfur and natural resources

Sulfur (S) is an abundant element in Earth's crust (McDonough and Sun, 1995; Rudnick and Gao, 2003), and highly reactive in different paragenetic conditions (Berner, 1984; Bottrell and Newton, 2006), resulting in over 1,100 different mineral species that contain S as an essential mineral forming component [(Rakovan, 2007; Lafuente et al., 2015; Krivovichev et al., 2023); https://rruff.info/ima/]. Sulfur redox sensitivity makes it an invaluable element for understanding Earth system redox evolution (Canfield et al., 2000, 2007; Hurtgen et al., 2005; Fike et al., 2006). Sulfate evaporite minerals have been used to constrain the chemistry and redox state of the ocean at different periods

* Corresponding author.
E-mail address: ekmoore@usgs.gov (E.K. Moore).

https://doi.org/10.1016/j.gca.2024.05.024
Received 25 June 2023; Accepted 22 May 2024
Available online 25 May 2024
0016-7037/Published by Elsevier Ltd.

of Earth history (Grotzinger and Kasting, 1993; Schröder et al., 2008), and the fractionation of different S isotopes [^{32}S, ^{33}S, ^{34}S, ^{36}S; ^{35}S is radiogenic and less relevant to long term geochemical records (Peters, 1959)] is associated with a wide range of different environmental and biological redox processes (Canfield, 2001; Behrens and Stelling, 2011; Cai et al., 2022). Moreover, the biogeochemical cycles of S and carbon (C) are directly involved in regulating atmospheric oxygen levels through the burial and oxidative weathering of organic matter and pyrite [FeS_2; (Berner, 1989, 2006)].

Sulfides (chemical species that contain S^{2-}) and sulfates (chemical species that contain SO_4^{2-}) have different redox driven isotope fractionations in a wide range of different systems including high temperature igneous systems, intermediate temperature hydrothermal systems, and low temperature sedimentary systems (Strauss, 1999; Seal, 2006). Fractionation values of the $\delta^{34}S$ isotope are generally higher for modern seawater sulfate and ancient sulfate containing marine evaporites compared to sulfides in meteorites, igneous rocks, fossil fuels, or pyrites from ancient or modern biogenic sources (Krouse, 1980; Seal et al., 2000). Of particular significance, the study of S isotope fractionation records has revealed the timing of the oxygenation of the atmosphere and ocean (Canfield, 1998; Farquhar et al., 2000; Farquhar and Wing, 2003; Sahoo et al., 2012; Luo et al., 2016). The reactivity of S in various redox states with many different chemical species allows S to form deposits in diverse systems across the geosphere (Simon and Ripley, 2011; Chou, 2012).

Sulfur is important in the formation of both inorganic and organic natural resources (Lundy, 1950; Williams and Keith, 1963). Specifically, the physicochemical properties of S strongly influence the formation of sulfide ores, many oxide ores, and element sulfur deposits (Malyshev and Malysheva, 2022). Connections between the sulfur cycle and ore deposits throughout Earth history in volcanogenic massive sulfide deposits, clastic-dominated Pb-Zn deposits, sediment hosted copper deposits, and Mississippi Valley-type deposits can all be linked to global sulfur cycling (Farquhar et al., 2010). Indeed, the redox state of aqueous S species (such as SO_4^{2-}, HSO_4^-, HS^-, H_2S, etc.) and S rich magmas plays a critical role in the formation of dozens of economically important ore deposit types such as copper (Cu), zinc (Zn), cobalt (Co), nickel (Ni), lead (Pb), gold (Au), silver (Ag), mercury (Hg), and platinum group elements (PGEs) (Vaughan, 2006; Simon and Ripley, 2011). Also of great importance to natural resource development, the redox transformations of S are involved in the diagenesis of marine organic matter, formation of energy resources, and subsequent S emissions for S incorporated in fossil fuels (Williams and Keith, 1963; Sinninghe Damste and De Leeuw, 1990; Chou, 2012).

1.2. Sulfur mineral chemistry redox record

Minerals are a vital record of environmental parameters, such as oxygen (O) fugacity in igneous systems, at the time of formation throughout Earth history (Wood and Virgo, 1989; Kress and Carmichael, 1991; Hazen et al., 2008; Birner et al., 2018). Sulfide minerals (containing reduced S) are more common in igneous systems than sulfate minerals (containing oxidized S), consisting mostly of pyrrhotite ($Fe_{1-x}S$) or pyrite (FeS_2), followed in abundance by chalcopyrite ($CuFeS_2$), pentlandite ($(Ni,Fe)_9S_8$), sphalerite (ZnS) or molybdenite (MoS_2) (Naldrett et al., 1967; Whitney and Stormer, 1983; Parat et al., 2011). The amounts of sulfides and sulfates forming from magmas indicate the predominate redox state as S^{2-} in sulfides and S^{6+} in sulfates, and can be used to evaluate the O fugacity of the system (Frost, 1991; Baker and Moretti, 2011). Oxidation and reduction reactions predominately occur under equilibrium conditions at high temperatures, while disequilibrium redox reactions are more common at lower temperatures, and S redox reactions or the exchange of S isotopes between reduced and oxidized S species generally results in the greatest S isotope fractionations (Seal, 2006). The complex redox chemistry of S minerals, and attendant isotopic fractionation, are used to trace the redox evolution of many different systems from magma to crust and atmosphere (Piccoli and Candela, 2002; Konecke et al., 2017; Sadove et al., 2019). Specifically, sedimentary pyrite $\delta^{34}S$ values have been used along with iron (Fe) speciation and trace metal concentrations to identify transitions in the S cycle associated with changing redox conditions in the Archean, Mesoproterozoic, and Phanerozoic oceans (Habicht et al., 2002; Leavitt et al., 2013; Crowe et al., 2014; Gilleaudeau and Kah, 2015).

In general, reduced sulfide is more associated with chalcophile and siderophile elements, while sulfate is more associated in salts with lithophile elements (Goldschmidt, 1937; Haldar, 2017). Sulfides (containing S^{2-}) and sulfates (containing S^{6+}) are abundant types of S minerals. However, the redox state of S is not known in hundreds of other S containing mineral species, mostly comprised of potential sulfides and sulfosalts [Mineral Evolution Database, https://rruff.info/evolution/; (Golden, 2019)]. The redox state of S in minerals can be determined using X-ray Absorption Near Edge Spectroscopy (XANES), or other methods, but the technique is not required for mineral characterization over time. Additionally, the redox state of S alone does not encapsulate the wide range of diverse chemical interactions among S-containing mineral species, limiting the potential use of S to further understand redox evolution. Because of the complex redox chemistry of S and coexistence with other redox-sensitive elements, many S-containing minerals have multiple potential element redox state combinations among the mineral's constituent elements that could result in a neutral charge. The redox states of other elements in S-containing minerals are important, but they can be stoichiometrically obscured due to the range of stable S valences that can exist in the mineral.

Sulfur is an essential element in biology, with many structural and functional roles that are linked to redox chemistry (Williams, 1981; Jelen et al., 2016). As a biological building block, S serves as a link between protein folds and metal cofactors, including mineral analogue FeS cofactors via the cysteine S-containing functional group (Beinert et al., 1997; Jordan et al., 2021). Some of the oldest known metabolic pathways utilize S species as an essential electron acceptor or donor (Shen et al., 2001, 2009; Westall et al., 2006; Philippot et al., 2007; Ueno et al., 2008; Bontognali et al., 2012; McLoughlin et al., 2012). Indeed, broad studies have shown that S redox chemistry is closely linked with carbon (C) cycling through time (Fike et al., 2015; Raven et al., 2019, 2021a). A greater understanding of the redox state of S in different depositional environments and time periods can help characterize biological utilization of S (Johnston, 2011), organic matter cycling (Raven et al., 2021b, 2023), and fossil fuel formation in a broad range of settings (Abubakar et al., 2022).

Sulfur can have very different chemical associations at different redox states and in different ionic species (Hawthorne et al., 2000), which can be characterized in deep-time mineral chemistry networks (Moore et al., 2023). In this study, we use mineral chemistry network analysis and both the weighted Mineral Element Electronegativity Coefficient of Variation ($wMEE_{CV}$) and weighted Mineral Element Electronegativity mean ($wMEE_{\mu}$) to investigate the different element interactions of S containing minerals. The $wMEE_{\mu}$ metric provides the mean of the electronegativity values for all elements in a given mineral's nominal chemical formula, while the $wMEE_{CV}$ metric provides the variation of the electronegativity values for all elements in a given mineral's nominal chemical formula. The $wMEE_{CV}$ metric has been used to identify global shifts in hard-soft acid-base chemistry of Earth's crust during the Proterozoic (Moore et al., 2022a). Mineral element electronegativity interactions represented by $wMEE_{\mu}$ and $wMEE_{CV}$ values, and differences in network associations between reduced and oxidized S can be employed to infer the redox state of S in minerals where the redox state is unknown, and to expand comprehension of the complexity of S mineral chemistry. This information can then be used to further understand the redox evolution of S-containing minerals throughout Earth history.

2. Methods

Bipartite mineral chemistry network analysis of S minerals was performed using the R package 'dragon' (Spielman and Moore, 2020). Data used in network analysis was obtained from the Mineral Evolution Database [MED; https://rruff.info/evolution/; (Golden, 2019), accessed February 3rd, 2020]. The MED contains the chemical formulas, characterized redox chemistry of mineral constituent elements, and the maximum known ages of all known mineral species. The dragon package can be launched in R by following the directions in the Readme file at https://github.com/sjspielman/dragon, and further details on using dragon are available in (Spielman and Moore, 2020). The mineral chemistry networks were constructed by selecting S as the focal element, and then initializing the network. Bipartite networks (a.k.a. bipartite graphs) contain two categories of nodes, in which nodes from category one are only connected to nodes from category two and vice versa [category one nodes are not connected to other category one nodes by network edges, and category two nodes are not connected to other category two nodes by network edges (Asratian et al., 1998)]. Social network analysis is a common use of bipartite networks to show affiliations between two groups of data (Wasserman and Faust, 1994).

The bipartite mineral chemistry networks constructed with dragon consist of mineral nodes and element nodes, in which the mineral nodes have network connections to all the constituent elements in that mineral's nominal chemical formula (network connections are referred to as "edges"). For example, the node representing the mineral pyrite FeS_2 has network edges connected to the element nodes for Fe and S. The default node position of the network layout is based on the force-directed Fruchterman-Reingold algorithm (Fruchterman and Reingold, 1991), which configures nodes based on the number of shared edges in the network. Further description of mineral chemistry networks constructed with dragon can be found in (Spielman and Moore, 2020). Separate S mineral chemistry networks were constructed to include minerals with maximum known ages of ≥3.2 Ga in one network and minerals with maximum known ages of ≥0 Ga in another network using the dragon age range slider function to compare differences between network communities including different S redox states. Mineral networks with separate nodes for each element redox state were constructed by selecting the "use separate nodes for each element redox" function in dragon. The ≥3.2 Ga time period was selected to examine minerals with maximum known ages that occurred before the tectonic transition period of 3.2 Ga to 2.5 Ga (Cawood et al., 2018; Brown et al., 2020; Windley et al., 2021) as compared to all minerals in the MED. The ≥3.2 Ga time period was also selected because $wMEE_{CV}$ values for the maximum known ages of S-containing minerals expand after 3.2 Ga.

The mineral nodes of each network are sized by the number of known localities in the MED to account for approximate crustal abundance of each mineral (Figs. 1, 2). The element nodes in the network in Fig. 1 are colored by Pauling electronegativity (Pauling, 1932) and the minerals are colored by $wMEE_{CV}$. The $wMEE_{CV}$ values and $wMEE_{\mu}$ values were calculated for each mineral species to investigate element interactions and redox relationships in the S mineral chemistry networks. The $wMEE_{CV}$ and $wMEE_{\mu}$ values were calculated using Pauling electronegativity (Pauling, 1932) values of each mineral's constituent elements, weighted by the number of each element in the nominal chemical formula of the mineral as described by (Moore et al., 2022a). Pauling scale electronegativity was chosen because the electronegativity values for each element are determined using multiple different covalent bonds for a given element. Using the number of each element in the nominal chemical formula in the mineral in the $wMEE_{CV}$ and $wMEE_{\mu}$ calculations accounts for the electronegativity influence that each element has in the mineral, such that an element that occurs multiple times in a mineral formula will have a greater electronegativity influence than an element that occurs once in the same mineral formula.

The $wMEE_{\mu}$ metric is calculated by taking the mean of the electronegativity values for all atoms in a given mineral's nominal chemical formula [e.g., cubanite; $CuFe_2S_3$; electronegativity of Cu = 1.90, Fe = 1.83, S = 2.58; $wMEE_{\mu}$ = mean of (1.90, 1.83, 1.83, 2.58, 2.58, 2.58) = 2.22]. The $wMEE_{CV}$ metric is calculated by taking the coefficient of variation of the electronegativity values for all elements in a given mineral's nominal chemical formula [e.g., cubanite; $CuFe_2S_3$; electronegativity of Cu = 1.90, Fe = 1.83, S = 2.58; $wMEE_{CV}$ = coefficient of variation of (1.90, 1.83, 1.83, 2.58, 2.58, 2.58) = 0.18]. Louvain community detection (Blondel et al., 2008) was performed for the networks in Fig. 2 using the igraph Package in R (Csardi and Nepusz, 2006) in order to identify associations between particular minerals, constituent

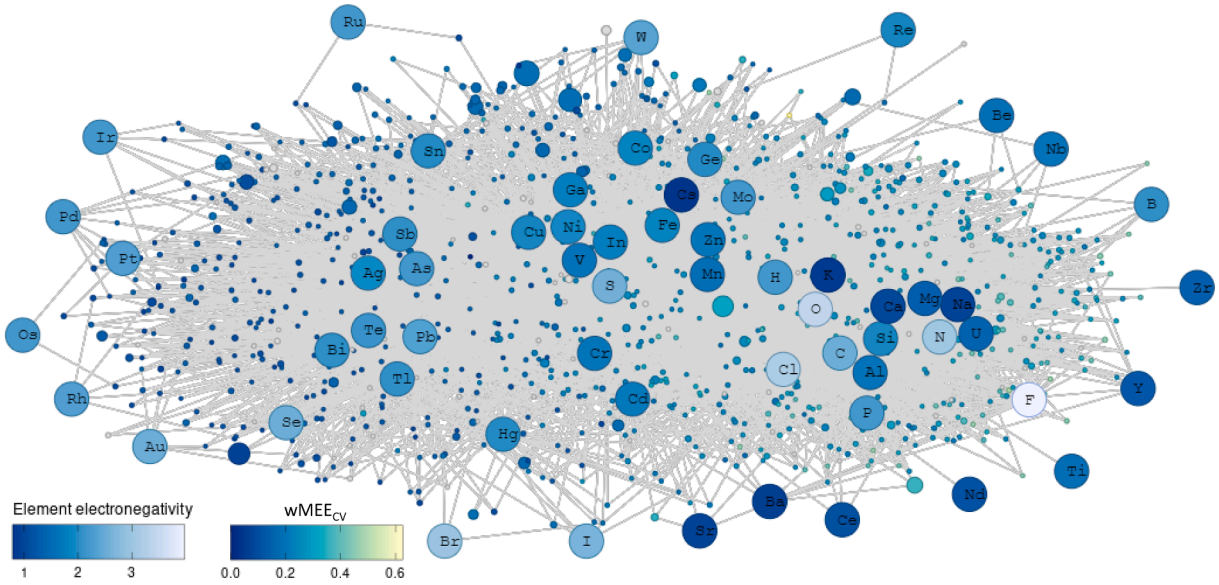

Fig. 1. Bipartite mineral chemistry network including all known S-containing minerals and their constituent elements. Element nodes are represented by blue color-scale circles with each element's chemical symbol, and are colored by Pauling scale electronegativity (Pauling, 1932). Mineral nodes are represented by small circles colored by weighted Mineral Element Electronegativity Coefficient of Variation ($wMEE_{CV}$). Network lines ("edges") connect mineral nodes to all of their constituent element nodes (e.g., pyrite – FeS_2 node has network edges connected to Fe and S). Mineral nodes are sized by the number of known localities. Node position of the default network layout configuration uses the force-directed Fruchterman-Reingold algorithm (Fruchterman and Reingold, 1991).

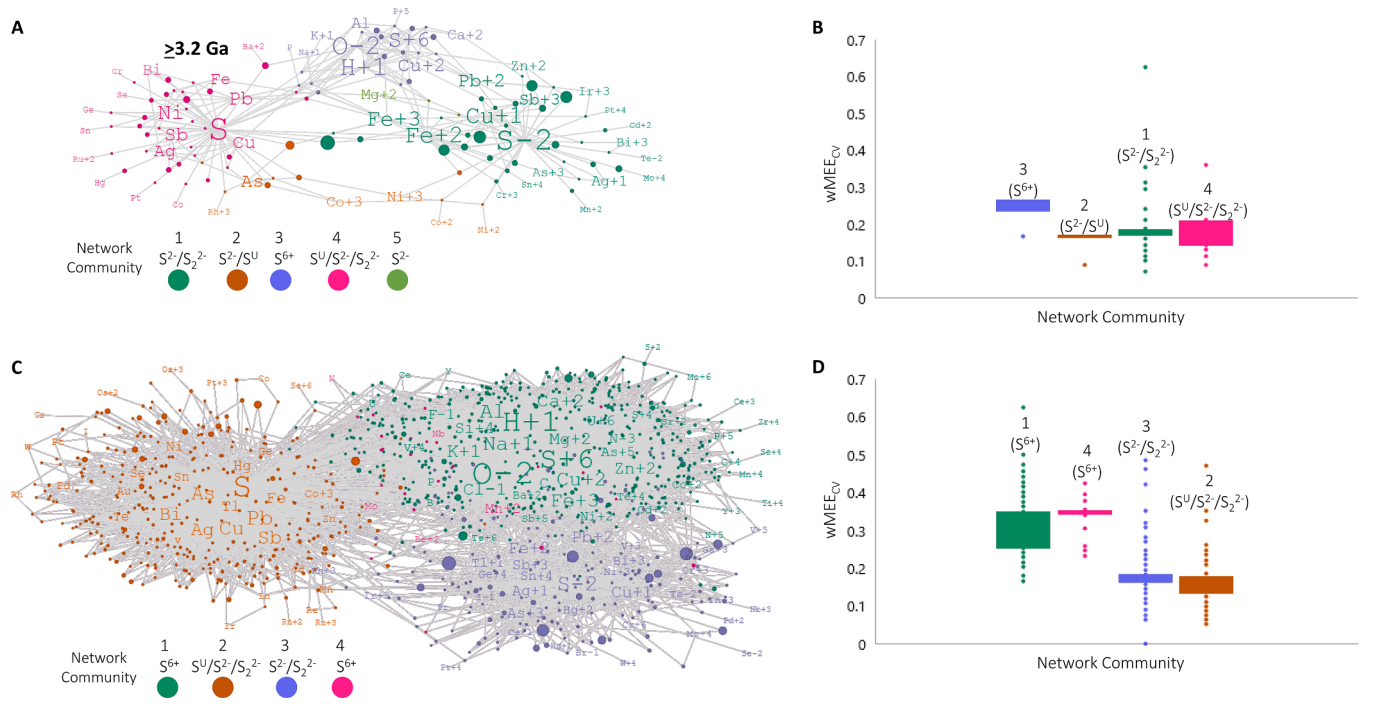

Fig. 2. (A) Sulfur mineral chemistry network including all known S-containing minerals with maximum known ages ≥ 3.2 Ga. Element nodes are separated by redox state. Mineral nodes are represented by circles and element nodes are represented by their chemical symbols. Mineral nodes are sized by the number of known localities in that time period, and element nodes are sized by the number of network edge connections. Mineral and element nodes are colored by Louvain community detection (Blondel et al., 2008). (B) Strip chart of weighted Mineral Element Electronegativity Coefficient of Variation ($wMEE_{CV}$) for each mineral in the Fig. 2A network separated by Louvain network community (Note: Network community 5 only included two data points and was excluded). (C) Same type of S mineral chemistry network as Fig. 2A, but including all known S-containing minerals and their constituent elements. (D) Strip chart of weighted Mineral Element Electronegativity Coefficient of Variation ($wMEE_{CV}$) for each mineral in the Fig. 2C network separated by Louvain network community.

elements, and element redox states. Louvain community detection optimizes modularity when identifying network node communities. Network element and mineral nodes in Fig. 2 are colored by Louvain community. Post-hoc Tukey tests comparing the $wMEE_{CV}$ values of Louvain network communities in the ≥3.2 Ga and ≥0 Ga networks (Fig. 2) were performed using R (R Core Team, 2021).

Geologic ages of mineral occurrences used in the sum of S mineral localities through time plot (Fig. 3A), $wMEE_{CV}$ through time plots (Fig. 3B, Fig. 4), S $wMEE_{\mu}$ vs. $wMEE_{CV}$ plot (Fig. 5A), and S closeness centrality vs. $wMEE_{CV}$ plot (Fig. 5B), were obtained from the MED [https://rruff.info/evolution/; (Golden, 2019)]. The $wMEE_{CV}$ statistical range (referred to throughout as the $wMEE_{CV}$ "range") was calculated for maximum known mineral ages (Fig. 3B) and all mineral occurrence ages (Fig. 4) in 0.5 Ga intervals with outlier data points excluded to reduce bias in the $wMEE_{CV}$ range (time intervals of 0.5 Ga were chosen to avoid gaps in $wMEE_{CV}$ data). Due to continental weathering processes, metamorphism, and the recycling of tectonic plates, there is a greater probability that older rocks and minerals will be lost or modified (Taylor and McLennan, 1995; Veizer and Mackenzie, 2014), resulting in preservation bias toward younger minerals. Sampling bias also takes place for economically significant minerals and harder minerals that are often less soluble and more resistant to weathering (Morrison et al., 2020), which is important for S-containing minerals whose hardnesses can vary between sulfides and sulfates (Czerewko et al., 2003). Diagenesis of mineral deposits can occur after host lithology formation, resulting in different potential ages of an altered mineral and its setting (Xu and Pruess, 2001). Despite potential biases that can occur due to preservation, age, and economic significance, expected pulses of increased mineralization are apparent during periods of known continental assembly [i.e., Kenorland 2.8–2.5 Ga, Columbia 2.0–1.8 Ga, Rodinia 1.3–0.9 Ga, Pannotia 0.54–0.5 Ga, and Pangea 0.4–0.3 Ga; (Voice et al., 2011; Hazen et al., 2019; Liu et al., 2019; Hummer et al., 2022)]. Additionally, global changes in $wMEE_{CV}$ values are observed at the same time periods for both maximum and minimum known ages of >200,000 mineral occurrences in the MED (Moore et al., 2022a). The global $wMEE_{CV}$ changes for both maximum and minimum known ages of mineral occurrences thus reveal the same shifts in crustal chemistry through time.

3. Results

3.1. Sulfur mineral chemistry network structure

The S mineral chemistry network is segregated into two sections based on electronegativity and hard soft acid base interactions. The left section of the network (Fig. 1) includes intermediate electronegativity soft acid/base elements that form low $wMEE_{CV}$ minerals (e.g., tungstenite, WS_2, $wMEE_{CV}$ = 0.051; miassite, $Rh_{17}S_{15}$, $wMEE_{CV}$ = 0.063), and the right section of the network includes high and low electronegativity hard acid/base elements (including O) that form high $wMEE_{CV}$ minerals (e.g., Arcanite, K_2SO_4, $wMEE_{CV}$ = 0.481; kogarkoite, Na_3SO_4F, $wMEE_{CV}$ = 0.498). The low $wMEE_{CV}$ minerals are largely sulfides or other minerals that do not contain O, and the high $wMEE_{CV}$ minerals predominately contain O (there are exceptions including the high $wMEE_{CV}$ calcium (Ca) sulfide oldhamite, CaS, $wMEE_{CV}$ = 0.624; and the high $wMEE_{CV}$ non-sulfate aluminum (Al) silicate sulfhydrylbystrite $Na_5K_2Ca[Al_6Si_6O_{24}](S_5)^{2-}(SH)^{-}$, $wMEE_{CV}$ = 0.410). First row transition metals are central in the network compared to most other elements, given that first row transition metals form many different sulfides or oxides at different redox states.

The S redox mineral chemistry network with element nodes separated by redox state illustrates that certain elements and certain element redox states only form minerals with particular S redox states (Fig. 2). Louvain community detection of the S redox mineral chemistry network

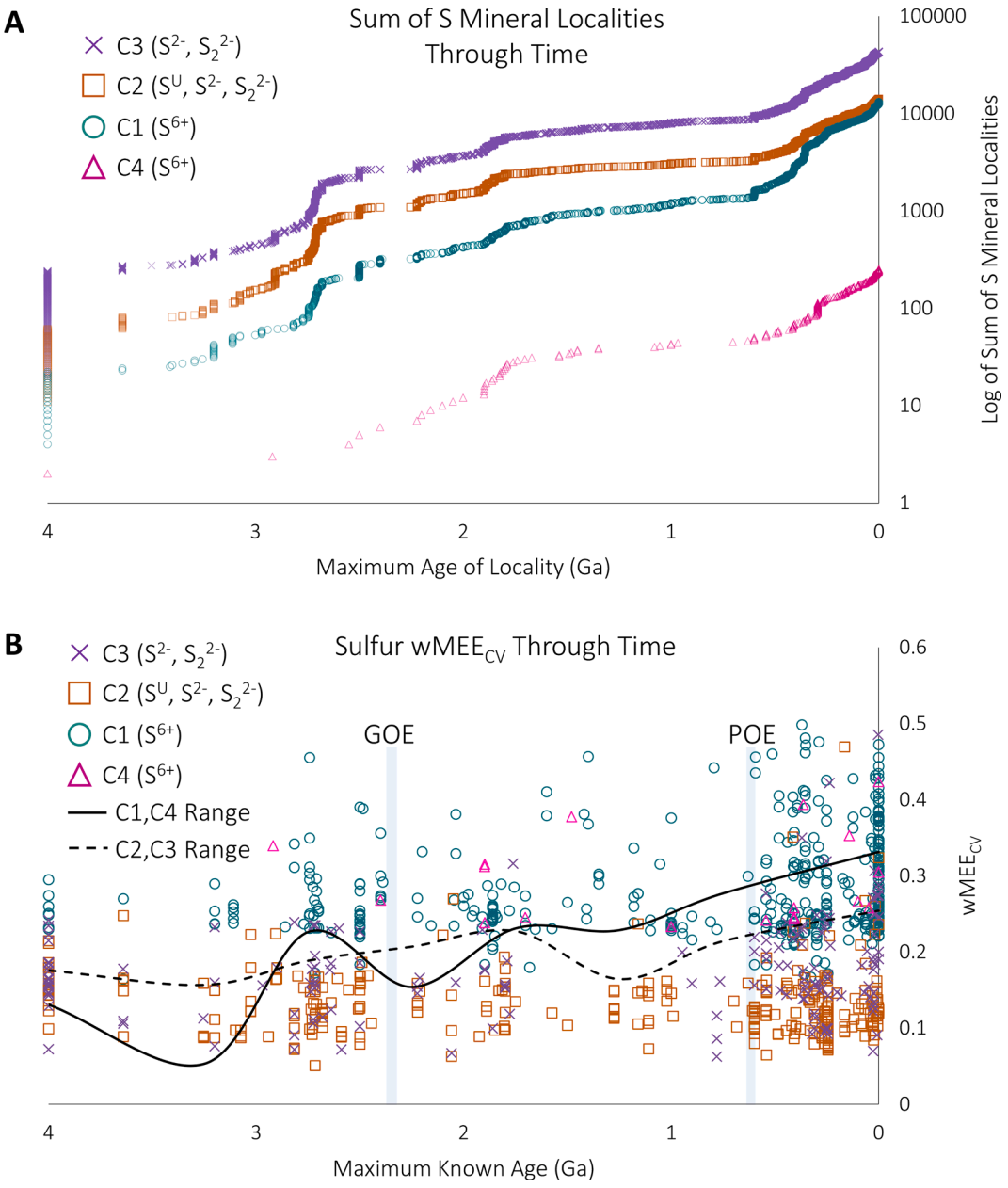

Fig. 3. Weighted Mineral Element Electronegativity Coefficient of Variation ($wMEE_{CV}$) maximum age and S mineral redox abundance through time. (A) Total number of S-containing mineral localities through time. The total mineral localities are separated by Fig. 2C ≥ 0 Ga S redox network Louvain community. (B) The $wMEE_{CV}$ values are plotted by maximum known mineral age of each S-containing mineral from 0 to 4 Ga. Data point colors and symbols are separated by Louvain network community from Fig. 2C. The solid plotted line represents the statistical range of $wMEE_{CV}$ values in 0.5 Ga intervals for communities 1 and 4, and the dashed plotted line represents the statistical range of $wMEE_{CV}$ values in 0.5 Ga intervals for communities 2 and 3. GOE = Great Oxygenation Event [2.4–2.3 Ga (Farquhar et al., 2000; Farquhar and Wing, 2003; Luo et al., 2016)]; POE = Proterozoic Oxygenation Event [0.63–0.55 Ga (Scott et al., 2008; Sahoo et al., 2012)].

including all minerals with maximum ages of ≥3.2 Ga, and with elements separated by redox state, shows that there are three main network communities and two minor network communities (Fig. 2A). The ≥3.2 Ga S redox network community 1 includes S^{2-} minerals, community 3 includes mainly S^{6+} minerals with fewer than ten total S^{4+} and S^{2+} minerals, and community 4 includes minerals in which the redox state of S is unknown (S^U). In the ≥3.2 Ga S redox network, community 2 includes nine minerals that contain either Ni^{3+}, Co^{3+}, or arsenic (As) with unknown redox state, and community 5 includes two minerals that contain Mg^{2+}. There are statistically significant differences by post-hoc Tukey Test between the $wMEE_{CV}$ values of community 1 vs. community 3, community 2 vs. community 3, and community 3 vs. community 4 in the ≥3.2 Ga S redox mineral chemistry network (Fig. 2B, Table 1). Conversely, there are not statistically significant differences by post-hoc Tukey Test between the $wMEE_{CV}$ values of community 1 vs. community 2, community 1 vs. community 4, and community 2 vs. community 4 in the ≥3.2 Ga S redox mineral chemistry network. The distinct network communities are due to the unique chemistry of the reduced, oxidized, and unknown S redox states which results in limited network overlap between the different redox state network nodes.

Similar to the ≥3.2 Ga S redox network, Louvain community detection of the S redox mineral chemistry network with elements separated by redox state including all minerals with maximum known ages ≥0 Ga shows that there are three main network communities and one minor network community (Fig. 2C). The ≥0 Ga S redox network community 1 includes S^{6+} minerals, community 2 includes S^U minerals,

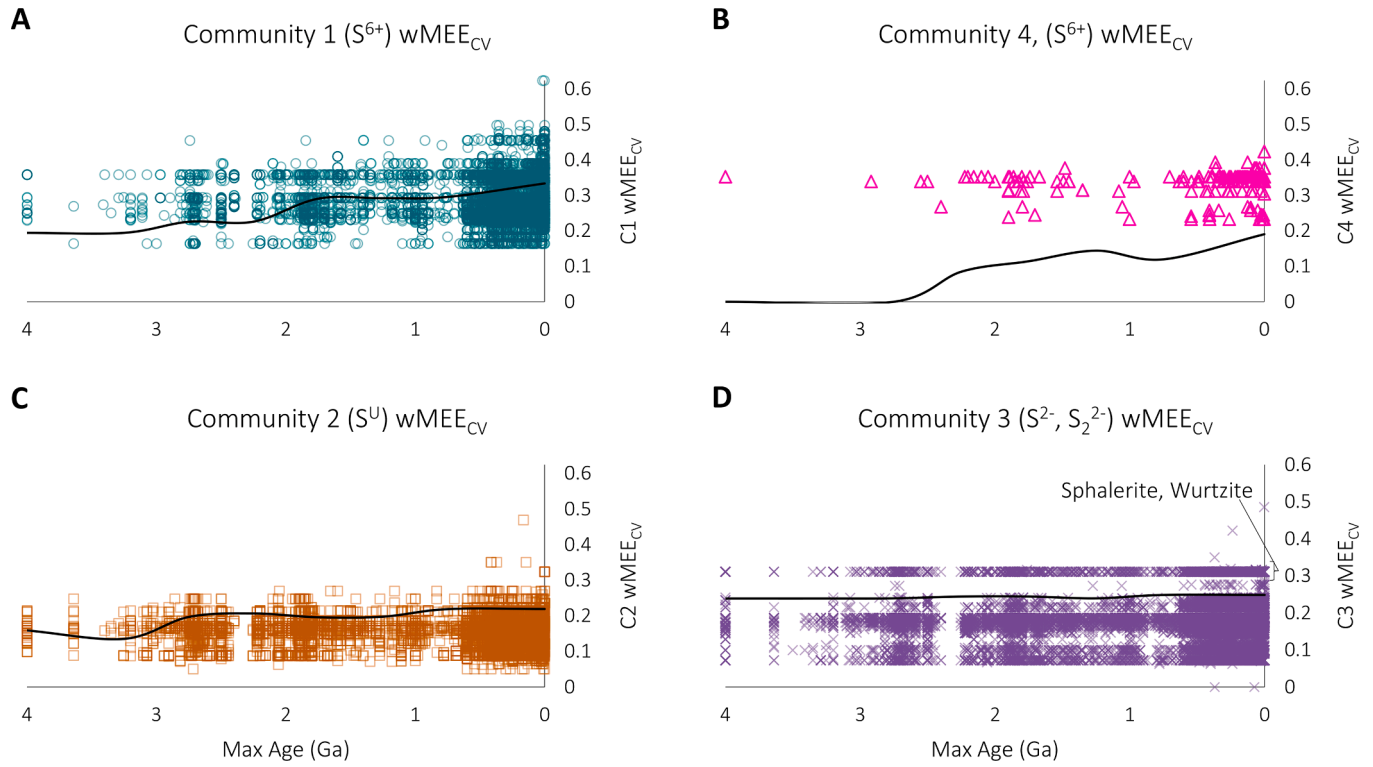

Fig. 4. Weighted Mineral Element Electronegativity Coefficient of Variation ($wMEE_{CV}$) locality ages through time. The $wMEE_{CV}$ values are plotted by maximum known mineral age from 0 to 4 Ga for each S-containing mineral locality from Fig. 2C ≥ 0 Ga S redox network Louvain community: (A) community 1 (13,083 localities); (B) community 4 (252 localities); (C) community 2 (14,129 localities); (D) community 3 (43,192 localities). The minerals sphalerite (ZnS) and wurtzite (ZnS) both have $wMEE_{CV}$ values of 0.311 and are labeled in Fig. 4D. The solid plotted line in each plot represents the statistical range of $wMEE_{CV}$ values in 0.5 Ga intervals for each community.

community 3 includes reduced S^{2-} or S_2^{2-} minerals, and community 4 is much smaller including minerals with Mn^{2+} and Be^{2+}. The ≥0 Ga S redox network is more connected than the ≥3.2 Ga S redox network, resulting in fewer distinct Louvain network communities in ≥0 Ga S redox network. In the ≥0 Ga S redox network, there are statistically significant differences by post-hoc Tukey Test between the $wMEE_{CV}$ values of nearly all the network communities (Fig. 2D, Table 1). Community 1 vs. community 4 is the only pair of two communities in the ≥0 Ga S redox network that do not have a statistically significant difference between their $wMEE_{CV}$ values by post-hoc Tukey Test.

3.2. Sulfur mineral electronegativity associations and redox implications

The cumulative sum of S-containing mineral localities through time for each network community shows rapid increases in S-containing mineral localities at 2.8 to 2.6 Ga, 1.9 to 1.8 Ga, 0.6 Ga to present day, and that minerals that contain S^{2-} have been found at the largest number of localities in the MED from deep time to present day (Fig. 3A). The $wMEE_{CV}$ values of mineral species in communities 1 and 4 from the ≥0 Ga S redox mineral chemistry network (containing S^{6+} minerals) generally expand through time, particularly after 3.2 Ga, based on the maximum known ages of S-containing mineral species (Fig. 3B). Communities 2 and 3 from the ≥0 Ga S redox network (contain S^{U} minerals and S^{2-} minerals, respectively) have more consistent mineral species $wMEE_{CV}$ values through time that largely overlap until 0.6 Ga, at which point community 3 includes a greater distribution of higher $wMEE_{CV}$ values than community 2. The distribution of $wMEE_{CV}$ values through time based on the maximum known ages of >70,000 S-containing mineral localities from around the globe also shows that the range of $wMEE_{CV}$ values expand the most through time for communities 1 and 4 (Fig. 4). The $wMEE_{CV}$ values largely overlap for communities 2 and 3 for S mineral localities as well (community 3: pyrite, FeS_2, $wMEE_{CV}$= 0.186; arsenopyrite, FeAsS, $wMEE_{CV}$ = 0.171). At <0.6 Ga community 2 includes smaller and larger $wMEE_{CV}$ values compared to >0.6 Ga, and community 3 includes larger values compared to >0.6 Ga, particularly 0.311, at many localities throughout most of Earth history corresponding to the abundant Zn sulfides sphalerite and wurtzite (Fig. 4D). The distribution of $wMEE_{CV}$ values through time for >70,000 S-containing mineral localities in the MED provides global trends of S mineral chemistry among different redox states and network communities.

The plot of $wMEE_{\mu}$ by $wMEE_{CV}$ shows that in general, minerals in network communities 2 and 3 with lower $wMEE_{\mu}$ (e.g. electronegativity mean) values also have lower $wMEE_{CV}$ (e.g. electronegativity variation) values than minerals in communities 1 and 4 (Fig. 5A). The $wMEE_{\mu}$ and $wMEE_{CV}$ values of communities 1 and 4 predominately overlap with each other, and are largely separated from communities 2 and 3, which largely overlap with each other. The majority of minerals in communities 1 and 4 also have higher network closeness centrality values than most of the minerals in communities 2 and 3, which indicates that communities 1 and 4 are more central in the S mineral chemistry network (Fig. 5B). The minerals with the highest closeness centrality values ranging from 3.6×10^{-4} to 3.9×10^{-4} include primarily minerals from community 1, which occur at the intersection of multiple network communities, and fewer minerals from communities 2, 3 and 4.

4. Discussion

4.1. Sulfur mineral chemistry network redox communities

As observed in previous mineral chemistry network studies involving other elements (Moore et al., 2018, 2020, 2022a,b,2023; Srivastava et al., 2021), the S mineral chemistry network consists of an oxidized hard acid-base section including high $wMEE_{CV}$ minerals, and a reduced soft acid-base section including low $wMEE_{CV}$ minerals (Fig. 1). Redox

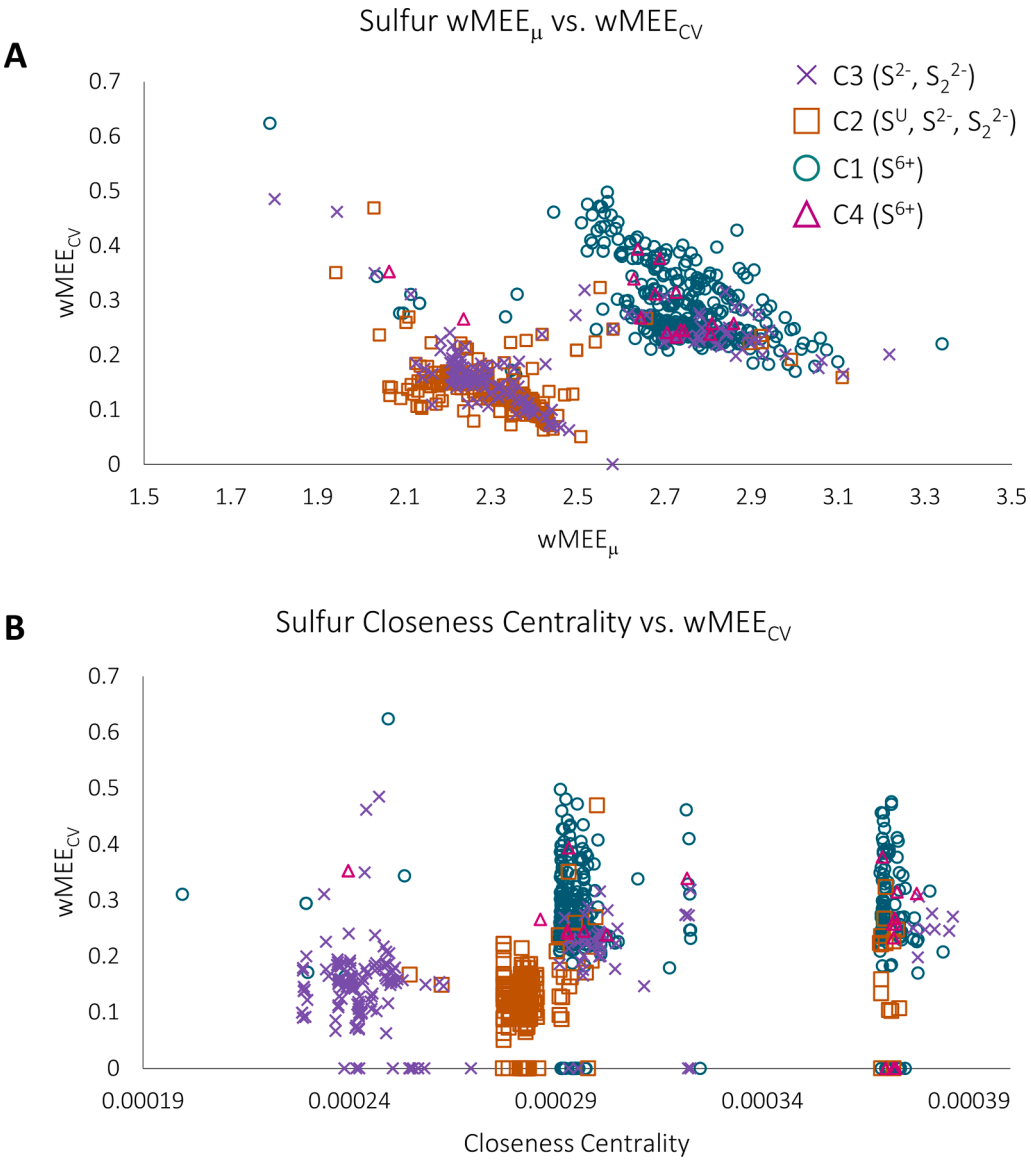

Fig. 5. (A) Plot of weighted Mean Mineral Element Electronegativity (wMEE$_\mu$) vs. weighted Mineral Element Electronegativity Coefficient of Variation (wMEE$_{CV}$) for each S-containing mineral species. (B) Plot of network closeness centrality vs. weighted Mineral Element Electronegativity Coefficient of Variation (wMEE$_{CV}$) for each mineral species in the Fig. 2C network with data points separated by Louvain network community.

Table 1
Tukey test results comparing wMEE$_{CV}$ values of Louvain communities for the ≥ 3.2 Ga S redox network in Fig. 2 and the ≥ 0 Ga S redox network in Fig. 3. Note: CI = confidence interval.

Age (Ga)	Cluster Comparison	Estimated effect size difference	95 % CI Lower bound	95 % CI Upper bound	Adjusted P-value
>3.2	2–1	−0.035	−0.110	0.040	0.607
>3.2	3–1	0.059	0.002	0.115	0.041
>3.2	4–1	−0.028	−0.076	0.020	0.420
>3.2	3–2	0.094	0.013	0.174	0.016
>3.2	4–2	0.007	−0.068	0.082	0.995
>3.2	4–3	−0.087	−0.144	−0.030	0.001
>0	2–1	−0.148	−0.160	−0.137	<0.0001
>0	3–1	−0.102	−0.116	−0.089	<0.0001
>0	4–1	0.016	−0.021	0.053	0.668
>0	3–2	0.046	0.031	0.061	<0.0001
>0	4–2	0.165	0.128	0.202	<0.0001
>0	4–3	0.119	0.081	0.156	<0.0001

sensitive first row transition metals [and molybdenum (Mo)] are associated with both reduced and oxidized S minerals in the S mineral chemistry network, with a wide range of wMEE$_{CV}$ values. The different mineral network interactions between S and transition metals reflect the prevalence of S-transition metal redox associations for both reduced and oxidized S in biochemistry and synthetic chemistry (Beinert, 2000; Eijsbouts et al., 2007; Emmett and Willis, 2015; Liang et al., 2016).

The separation of different network communities and their shared node connections becomes much more apparent in the S redox mineral chemistry networks with each element node separated by redox state (Fig. 2). Indeed, the similarities and differences in element associations among each network community can be used to understand redox chemistry in minerals where the redox state is not known. The statistically significant difference by post-hoc Tukey test between the wMEE$_{CV}$ values of community 1 vs. community 3 in the ≥3.2 Ga S redox network represents the different mineral element electronegativity associations among minerals that contain S^{2-} (community 1 – reduced minerals) vs. S^{6+} (community 3 – oxidized minerals; Fig. 2A, 2B, Table 1). Conversely, there is no statistically significant difference between the wMEE$_{CV}$ values of ≥3.2 Ga S redox network communities 1 (S^{2-}, S_2^{2-}), 2 (S^{2-} and

S^U), and 4 (S^U), indicating that the minerals in communities 2 and 4 predominately contain reduced S as sulfide (S^{2-}) or persulfide (S_2^{2-}). This finding is reasonable given that both S^{2-} and S^U minerals do not contain O and the similarity of network element associations within the communities (Fig. 2). If it is assumed that the vast majority of S^U minerals actually contain reduced S, as indicated by $wMEE_{CV}$ values, network associations, and the absence of O in S^{2-}- and S^U-containing minerals, then oxidized S-containing mineral species make up a much smaller fraction of total S-containing mineral species and localities at ≥3.2 Ga (note: abundant minerals in the environment by volume also make up large percentages of S-containing mineral localities: pyrite-10.68%; chalcopyrite-8.97%; baryte-3.47%; gypsum-2.11%; and anhydrite-0.61%). This observation is expected given the reducing conditions in the geosphere and atmosphere during the Hadean, Eoarchean, and Paleoarchean (Shaw, 2008; Trail et al., 2011; Morrison et al., 2018), with an important exception occurring in 3.47 Ga North Pole barytes where oxidized sulfur (i.e. sulfate) was abundant enough for baryte deposits to form that included preserved isotopic evidence of sulfate reduction (Shen and Buick, 2004).

Various comprehensive studies have identified 3.2 Ga to 2.5 Ga as a period of tectonic transition prior to the onset of Wilson Cycle plate tectonics (Cawood et al., 2018; Brown et al., 2020; Windley et al., 2021). The $wMEE_{CV}$ values for S^{6+} minerals expands after 3.2 Ga (Fig. 3B, 4A), and the majority of minerals with maximum known ages between 3.2 and 2.5 Ga have $wMEE_{CV}$ values below 0.3 and are either sulfates with complex chemical formulas or sulfides. The S-containing minerals that have been observed at the largest number of localities from 3.2 to 2.5 Ga are pyrite (FeS_2), chalcopyrite ($CuFeS_2$), pyrrhotite (Fe_7S_8), sphalerite (ZnS), and galena (PbS). After 3.2 Ga, the transition of tectonic regime shift, and stepwise oxygenation of the atmosphere contributes to the origination and preservation of new S-containing mineral species, which expands the different element associations and redox chemistry diversity in the S mineral chemistry network. The network communities in the ≥0 Ga S redox network that include minerals containing oxidized S^{6+} (communities 1 and 4) on average have higher $wMEE_{CV}$ values and higher $wMEE_{\mu}$ values than the network community that contains reduced S (community 3; Fig. 2C, 5A), in agreement with previously observed $wMEE_{CV}$ trends comparing oxidized and reduced minerals (Moore et al., 2022a). There is substantial overlap between the $wMEE_{CV}$ values and $wMEE_{\mu}$ values of the ≥0 Ga S redox communities 3 and 2, which include S^{2-}-, S_2^{2-}-, and S^U-containing minerals, respectively (Fig. 2D, 5A). As with the ≥3.2 Ga S redox network, this indicates that the mineral species in community 2 (S^U) of the ≥0 Ga S redox network predominately contain reduced S. Additionally, there is a limited number of various S^U minerals in ≥0 Ga S redox network community 2 that contain the persulfide ion (S_2^{2-}) in which S is present in the S^- oxidation state including the highly abundant mineral pyrite (Paszkowicz and Leiro, 2005).

Sulfur mineral chemistry network analysis and associated element electronegativity interactions closely align with the known redox states of S-containing minerals that include or do not include O (Sato, 1960; Nordstrom, 1982; Ivanov, 1983; de Hoog et al., 2004). However, the majority of mineral species (~56%) with unknown redox state in community 2 of the ≥0 Ga S redox network are sulfosalts (Supplementary Table S1), which are difficult to characterize in terms of redox state (Moëlo et al., 2008). Many of the remaining ≥0 Ga S redox network community 2 sulfide minerals (Fig. 2C), that are not classified as sulfosalts, also include complex anions (Supplementary Table S1) that are characteristic of sulfosalts (Makovicky, 2019). Network community detection, $wMEE_{CV}$ calculations, and $wMEE_{\mu}$ calculations provide substantial support that sulfosalts and other S-containing minerals in which the redox state is unknown contain reduced S^{2-} or S_2^{2-}, given the similarity between $wMEE_{CV}$ values of S^U minerals and reduced-S minerals and the dissimilarity between $wMEE_{CV}$ values of S^U minerals and S^{6+} containing minerals.

4.2. Sulfur mineral redox evolution

The increasing range of $wMEE_{CV}$ values for ≥0 Ga S redox network communities 1 and 4, which almost exclusively include oxidized S^{6+}-containing minerals (Figs. 3-5), generally coincides with Earth surface oxygenation through time recorded in the S geochemical record (Canfield, 1998; Canfield et al., 2000, 2007; Farquhar et al., 2000; Hurtgen et al., 2005; Fike et al., 2006), and the oxidation of Earth's shallow crust embedded in the manganese (Mn) mineral record (Hummer et al., 2022). Greater chemical complexity of minerals with S-O bonds vs. minerals without S-O bonds also allows for a wider range of $wMEE_{CV}$ values for oxidized S^{6+}-containing minerals. Indeed, the proportion of S^{6+}-containing minerals (≥0 Ga S redox network communities 1 and 4) occurring in sediments due to Earth surface oxidation increases through time, particularly during the Phanerozoic [MED, https://rruff.info/evolution/; (Golden, 2019)]. The rising occurrence and preservation of ≥0 Ga S redox network community 1 mineral localities with $wMEE_{CV}$ values >0.35 from the late Mesoproterozoic to present day as compared to previous geologic eras, mainly consists of sulfate minerals that contain alkali metals and alkaline Earth metals. These alkali metal and alkaline Earth metal sulfate minerals formed with increased oxidative continental weathering and subsequent mineralization increasing from the late Proterozoic to Phanerozoic (Jambor et al., 2000; Berner, 2004; Canfield, 2005; Halevy et al., 2012).

Although the range of $wMEE_{CV}$ values stays more consistent for ≥0 Ga S redox network communities 2 and 3 as compared to community 1, the substantial overlap between $wMEE_{CV}$ values in communities 2 and 3 through time strongly indicates that community 2 minerals contain reduced S^{2-} or S_2^{2-} as do community 3 minerals (Figs. 3B, 4). The most common minerals of community 3 whose $wMEE_{CV}$ values do not overlap with community 2 are sphalerite (ZnS) and wurtzite (ZnS), two common and economically important sources of Zn (Scott and Barnes, 1972; Ye et al., 2011). The abundance of oxidized S^{6+}-containing minerals in community 1 does sharply increase in the Phanerozoic, but community 3 mineral localities, which almost exclusively contain S^{2-} or S_2^{2-}, make up the majority of S-containing mineral localities in the MED (Fig. 3A). If it is assumed that community 2 minerals also contain S^{2-} or S_2^{2-} (e.g., enargite, Cu_3AsS_4, $wMEE_{CV} = 0.149$; pyrargyrite, Ag_3SbS_3, $wMEE_{CV} = 0.150$; bismuthinite, Bi_2S_3, $wMEE_{CV} = 0.130$), as supported by their network chemical associations and $wMEE_{CV}$ values, then reduced S-containing minerals make up approximately 81% of S-containing minerals in the MED (communities 2+3 localities = 57,321; total localities = 70,656). The prevalence of reduced S-containing mineral localities aligns with the typically low δO_2 values of the upper mantle and lower crust (McCammon and Kopylova, 2004; Galvez and Jaccard, 2021), and reinforces the connection between the oxidation state of the mantle and Earth surface processes (McCammon, 2005; Gaillard et al., 2015).

Community 3 mineral localities that are known to contain reduced S and community 2 mineral localities that are predicted to contain reduced S, increase substantially during the Phanerozoic as well, despite the increase in oxidative weathering (Canfield and Teske, 1996; Berner et al., 2003; Halverson and Hurtgen, 2007) and disappearance of redox sensitive minerals from placer deposits during this period (Hazen et al., 2011; Johnson et al., 2014; Agarwal and Sreenivas, 2021). Sulfur-containing mineral localities increase through time in part due to preservation bias of younger material, and the formation and preservation of many reduced S mineral localities indicates that many of these minerals formed in recent reducing environments that are not subject to wide changes in redox conditions. Indeed, one of the most prominent localities for sulfosalt minerals is the Lengenbach deposit in the Binn Valley of the Swiss Alps that has a relatively recent age of 0.06 Ga (Nowacki et al., 1961; Hofmann and Knill, 1996). The prevalence of S^{2-} minerals in magmatic source material, and the formation and preservation of reduced minerals from igneous source rocks due to supercontinent assembly and orogenesis (Hazen et al., 2019; Liu et al., 2019; Santosh and Groves, 2022) are likely major contributing factors to S^{2-}- or S_2^{2-}-

containing minerals accounting for the majority of S-containing mineral localities in the MED.

4.3. Sulfur redox convergence

Despite the greater number of S-containing mineral species that also contain O resulting in greater network closeness centrality for S^{6+}-containing minerals (Fig. 5), the total number of mineral localities is greater for reduced S-containing minerals. This is contrary to the total mineral localities in the MED (including S-containing minerals and all non S-containing minerals), the majority of which contain O. In fact, assuming that ≥0 Ga S redox network community 2 mineral localities contain reduced S, then the vast majority of non-O-containing mineral localities in the MED are reduced S-containing minerals (~75%).

While pyrite is the largest sink of reduced sedimentary S (Berner and Raiswell, 1983), there are many other reduced S minerals and reduced S in organic matter that can contribute to the reduced S reservoir in the geosphere, including sulfosalts and other minerals with network predicted S^{2-} or S_2^{2-} redox state (Figs. 2-4). The expansion of S $wMEE_{CV}$ values through time for S^{6+} and S^{U} minerals represents redox convergence of weathered S as an electron donor between the oxidizing surface and reducing geosphere as S is transported and mineralized. Indeed, oxidatively weathered and mobilized metal and other nutrient ions, reflecting the expansion of the marine sulfate reservoir and subsequent sulfate reduction (Canfield and Raiswell, 1999), can then be utilized by microbial communities or transported to reducing environments to potentially form minerals with reduced S.

Sulfur mineral chemistry redox intersection through time aligns with the syngenesis of sulfide ore from different sources (Temple and Le Roux, 1964; Temple, 1964), and the convergence of environmental boundary conditions that contributed to the evolution of biogeochemical cycles (Moore et al., 2017; Goldford et al., 2019). Moreover, the sequential evolution of S cycling enzymes involved in sulfide oxidation, sulfate-thiosulfate oxidation/reduction, and organic S metabolism across the biosphere reflects the redox state of early Earth from the Archean to Proterozoic (Mateos et al., 2023). The prevalence of S^{2-} mineral localities throughout Earth history illustrates the prominence of reduced S in the geosphere as an important metabolic substrate, component in organic matter diagenesis (Sinninghe Damste and De Leeuw, 1990; Werne et al., 2004), a crucial source of electrons in microbial metabolic pathways (Canfield, 2001; Fike et al., 2015), and a building block in protein metal binding complexes (Vahrenkamp, 1975; Williams, 1981).

5. Conclusions

The oxidation of Earth's crust and cycling of elements in the environment can be traced through the mineral record in deep-time. Sulfur readily exchanges between the geosphere and biosphere, and S is one of the most common mineral-forming elements, with complex redox chemistry that results in diverse mineral element associations. Mineral chemistry network analysis shows that the S mineral chemistry network consists of an oxidized hard acid-base section including high $wMEE_{CV}$ minerals, and a reduced soft acid-base section including low $wMEE_{CV}$ minerals. The expanding range of $wMEE_{CV}$ values for S^{6+} community minerals through time accord with Earth surface oxidation, increased oxidative continental weathering, and the expansion of the marine sulfate pool from the Proterozoic to Phanerozoic resulting in redox convergence of oxidized and reduced S minerals. The direct overlap between the $wMEE_{CV}$ values of the S redox network S^{U} community, primarily composed of sulfosalts, and the $wMEE_{CV}$ values of the S^{2-} community, strongly indicates that S^{U} community minerals with unknown redox state contain reduced S^{2-} or S_2^{2-}. Assuming that S^{U} community minerals contain reduced S (e.g., enargite, Cu_3AsS_4, $wMEE_{CV}$ = 0.149; pyrargyrite, Ag_3SbS_3, $wMEE_{CV}$ = 0.150; bismuthinite, Bi_2S_3, $wMEE_{CV}$ = 0.130), based on network chemical associations and $wMEE_{CV}$ values, then reduced S-containing minerals make up the vast majority of S-containing mineral localities in the MED, despite the fact that the majority of all mineral localities in the MED (both S-containing and non-S-containing minerals) are comprised of O-containing minerals. Additionally, reduced S-containing minerals make up the majority of all non-O containing minerals in the MED, illustrating the role of reduced S in the geosphere as an important reservoir of reduced inorganic materials, a component in organic matter cycling, and a crucial substrate and source of electrons in global biogeochemical cycles and associated microbial metabolic networks.

Data availability

Data presented in this manuscript can be accessed from the Mineral Evolution Database (http://rruff.info/evolution/). dragon is freely available as an open-source R package and is accessible from CRAN (https://cran.r-project.org/) to analyze data from the Mineral Evolution Database.

CRediT authorship contribution statement

Eli K. Moore: . **Joseph E. Diedolf IV:** Writing – review & editing, Visualization. **Shaunna M. Morrison:** Writing – review & editing, Data curation. **Daniel R. Hummer:** Writing – review & editing, Data curation.

Declaration of competing interest

The authors declare that they have no known competing financial interests or personal relationships that could have appeared to influence the work reported in this paper.

Acknowledgements

We thank Joshua J. Golden for his assistance in working with the Mineral Evolution Database. We thank Andrew Masterson (U.S. Geological Survey), Aaron Jubb (U.S. Geological Survey), Robert Downs and Robert Hazen for their comments and input as well. This work was supported financially by the Energy Resources Program of the U.S. Geological Survey. Any use of trade, firm, or product names is for descriptive purposes only and does not imply endorsement by the U.S. Government. This project was also funded in part by NSF EAR2020520, NASA Astrobiology Institute (Cycle 8) ENIGMA: Evolution of Nanomachines In Geospheres and Microbial Ancestors (80NSSC18M0093), and the 4D Deep-Time Data Driven Initiative at the Carnegie Institution for Science.

Appendix A. Supplementary material

We include in the supplementary material a data table of the ≥0 Ga sulfur redox network (Fig. 2C) Louvain community 2 mineral Dana classification and Strunz classification for minerals that do not have available Dana classification. Supplementary material to this article can be found online at https://doi.org/10.1016/j.gca.2024.05.024.

References

Abubakar, Y., Taylor, K.G., Coker, V., Wogelius, R.A., van Dongen, B.E., 2022. Fundamental controls on organic matter preservation in organic- and sulfur-rich hydrocarbon source rocks. Mar. Pet. Geol. 141, 105684.

Agarwal, D.K., Sreenivas, B., 2021. An appraisal of uranium deposits of India and their style of deposition with reference to the Paleoproterozoic great oxidation event. Int. Geol. Rev. 63, 571–584.

Asratian, A.S., Denley, T.M.J., Häggkvist, R., 1998. Bipartite Graphs and their Applications. Cambridge University Press.

Baker, D.R., Moretti, R., 2011. Modeling the Solubility of Sulfur in Magmas: A 50-Year Old Geochemical Challenge. Rev. Mineral. Geochem. 73, 167–213.

Behrens, H., Stelling, J., 2011. Diffusion and Redox Reactions of Sulfur in Silicate Melts. Rev. Mineral. Geochem. 73, 79–111.
Beinert, H., 2000. A tribute to sulfur. Eur. J. Biochem. 267, 5657–5664.
Beinert, H., Holm, R.H., Münck, E., 1997. Iron-Sulfur Clusters: Nature's Modular, Multipurpose Structures. Science 277, 653–659.
Berner, R.A., 1984. Sedimentary pyrite formation: An update. Geochim. Cosmochim. Acta 48, 605–615.
Berner, R.A., 1989. Biogeochemical cycles of carbon and sulfur and their effect on atmospheric oxygen over phanerozoic time. Glob. Planet. Change 1, 97–122.
Berner, R.A., 2004. A model for calcium, magnesium and sulfate in seawater over Phanerozoic time. Am. J. Sci. 304, 438–453.
Berner, R.A., 2006. GEOCARBSULF: A combined model for Phanerozoic atmospheric O2 and CO2. Geochim. Cosmochim. Acta 70, 5653–5664.
Berner, R.A., Beerling, D.J., Dudley, R., Robinson, J.M., Wildman, R.A., 2003. Phanerozoic Atmospheric Oxygen. Annu. Rev. Earth Planet. Sci. 31, 105–134.
Berner, R.A., Raiswell, R., 1983. Burial of organic carbon and pyrite sulfur in sediments over phanerozoic time: a new theory. Geochim. Cosmochim. Acta 47, 855–862.
Birner, S.K., Cottrell, E., Warren, J.M., Kelley, K.A., Davis, F.A., 2018. Peridotites and basalts reveal broad congruence between two independent records of mantle fO2 despite local redox heterogeneity. Earth Planet. Sci. Lett. 494, 172–189.
Blondel, V.D., Guillaume, J.-L., Lambiotte, R., Lefebvre, E., 2008. Fast unfolding of communities in large networks. J. Stat. Mech: Theory Exp. 2008, P10008.
Bontognali, T.R.R., Sessions, A.L., Allwood, A.C., Fischer, W.W., Grotzinger, J.P., Summons, R.E., Eiler, J.M., 2012. Sulfur isotopes of organic matter preserved in 3.45-billion-year-old stromatolites reveal microbial metabolism. Proc. Natl. Acad. Sci. 109, 15146–15151.
Bottrell, S.H., Newton, R.J., 2006. Reconstruction of changes in global sulfur cycling from marine sulfate isotopes. Earth Sci. Rev. 75, 59–83.
Brown, M., Johnson, T., Gardiner, N.J., 2020. Plate Tectonics and the Archean Earth. Annu. Rev. Earth Planet. Sci. 48, 291–320.
Cai, C., Li, H., Li, K., Wang, D., 2022. Thermochemical sulfate reduction in sedimentary basins and beyond: A review. Chem. Geol. 607, 121018.
Canfield, D.E., 1998. A new model for Proterozoic ocean chemistry. Nature 396, 450–453.
Canfield, D.E., 2001. Biogeochemistry of Sulfur Isotopes. Rev. Mineral. Geochem. 43, 607–636.
Canfield, D.E., 2005. The early history of atmospheric oxygen: homage to robert M. Garrels. Annu. Rev. Earth Planet. Sci. 33, 1–36.
Canfield, D.E., Habicht, K.S., Thamdrup, B., 2000. The Archean Sulfur Cycle and the Early History of Atmospheric Oxygen. Science 288, 658–661.
Canfield, D.E., Poulton, S.W., Narbonne, G.M., 2007. Late-Neoproterozoic Deep-Ocean Oxygenation and the Rise of Animal Life. Science 315, 92–95.
Canfield, D.E., Raiswell, R., 1999. The evolution of the sulfur cycle. Am. J. Sci. 299, 697–723.
Canfield, D.E., Teske, A., 1996. Late Proterozoic rise in atmospheric oxygen concentration inferred from phylogenetic and sulphur-isotope studies. Nature 382, 127–132.
Cawood, P.A., Hawkesworth, C.J., Pisarevsky, S.A., Bruno, D., Capitanio, F.A., Oliver, N., 2018. Geological archive of the onset of plate tectonics. Philos. Trans. r. Soc. Math. Phys. Eng. Sci. 376, 20170405.
Chou, C.-L., 2012. Sulfur in coals: A review of geochemistry and origins. Int. J. Coal Geol. 100, 1–13.
Crowe, S.A., Paris, G., Katsev, S., Jones, C., Kim, S.-T., Zerkle, A.L., Nomosatryo, S., Fowle, D.A., Adkins, J.F., Sessions, A.L., Farquhar, J., Canfield, D.E., 2014. Sulfate was a trace constituent of Archean seawater. Science 346, 735–739.
Csardi G. and Nepusz T. (2006) The igraph software package for complex network research. *InterJournal* **Complex Systems**, 1695.
Czerewko, M.A., Cripps, J.C., Reid, J.M., Duffell, C.G., 2003. Sulfur species in geological materials—sources and quantification. Cem. Concr. Compos. 25, 657–671.
de Hoog, J.C.M., Hattori, K.H., Hoblitt, R.P., 2004. Oxidized sulfur-rich mafic magma at Mount Pinatubo, Philippines. Contrib. Mineral. Petrol. 146, 750–761.
Eijsbouts, S., Mayo, S.W., Fujita, K., 2007. Unsupported transition metal sulfide catalysts: From fundamentals to industrial application. Appl. Catal. A 322, 58–66.
Emmett, E.J., Willis, M.C., 2015. The Development and Application of Sulfur Dioxide Surrogates in Synthetic Organic Chemistry. Asian J. Org. Chem. 4, 602–611.
Farquhar, J., Bao, H., Thiemens, M., 2000. Atmospheric Influence of Earth's Earliest Sulfur Cycle. Science 289, 756–758.
Farquhar, J., Wing, B.A., 2003. Multiple sulfur isotopes and the evolution of the atmosphere. Earth Planet. Sci. Lett. 213, 1–13.
Farquhar, J., Wu, N., Canfield, D.E., Oduro, H., 2010. Connections between Sulfur Cycle Evolution, Sulfur Isotopes, Sediments, and Base Metal Sulfide Deposits. Econ. Geol. 105, 509–533.
Fike, D.A., Grotzinger, J.P., Pratt, L.M., Summons, R.E., 2006. Oxidation of the Ediacaran Ocean. Nature 444, 744–747.
Fike, D.A., Bradley, A.S., Rose, C.V., 2015. Rethinking the Ancient Sulfur Cycle. Annu. Rev. Earth Planet. Sci. 43, 593–622.
Frost, B.R., 1991. Introduction to oxygen fugacity and its petrologic importance. Rev. Mineral. Geochem. 25, 1–9.
Fruchterman, T.M.J., Reingold, E.M., 1991. Graph drawing by force-directed placement. Softw. Pract. Exp. 21, 1129–1164.
Gaillard, F., Scaillet, B., Pichavant, M., Iacono-Marziano, G., 2015. The redox geodynamics linking basalts and their mantle sources through space and time. Chem. Geol. 418, 217–233.
Galvez, M.E., Jaccard, S.L., 2021. Redox capacity of rocks and sediments by high temperature chalcometric titration. Chem. Geol. 564, 120016.
Gilleaudeau, G.J., Kah, L.C., 2015. Heterogeneous redox conditions and a shallow chemocline in the Mesoproterozoic ocean: Evidence from carbon–sulfur–iron relationships. Precambr. Res. 257, 94–108.
Golden, J.J., 2019. Mineral evolution database: Data model for mineral age associations. MS Thesis, Department of Geosciences. University of Arizona.
Goldford, J.E., Hartman, H., Marsland, R., Segrè, D., 2019. Environmental boundary conditions for the origin of life converge to an organo-sulfur metabolism. Nat. Ecol. Evol. 3, 1715–1724.
Goldschmidt V. M. (1937) The principles of distribution of chemical elements in minerals and rocks. The seventh Hugo Müller Lecture, delivered before the Chemical Society on March 17th, 1937. *J. Chem. Soc. Resumed*, 655–673.
Grotzinger, J.P., Kasting, J.F., 1993. New Constraints on Precambrian Ocean Composition. J. Geol. 101, 235–243.
Habicht, K.S., Gade, M., Thamdrup, B., Berg, P., Canfield, D.E., 2002. Calibration of Sulfate Levels in the Archean Ocean. Science 298, 2372–2374.
Haldar S. K. (2017) Chapter 1 - Introduction. In *Platinum-Nickel-Chromium Deposits* (ed. S. K. Haldar). Elsevier. pp. 1–35.
Halevy, I., Peters, S.E., Fischer, W.W., 2012. Sulfate Burial Constraints on the Phanerozoic Sulfur Cycle. Science 337, 331–334.
Halverson, G.P., Hurtgen, M.T., 2007. Ediacaran growth of the marine sulfate reservoir. Earth Planet. Sci. Lett. 263, 32–44.
Hawthorne, F.C., Krivovichev, S.V., Burns, P.C., 2000. The Crystal Chemistry of Sulfate Minerals. Rev. Mineral. Geochem. 40, 1–112.
Hazen, R.M., Papineau, D., Bleeker, W., Downs, R.T., Ferry, J.M., McCoy, T.J., Sverjensky, D.A., Yang, H., 2008. Mineral evolution. Am. Mineral. 93, 1693–1720.
Hazen, R.M., Bekker, A., Bish, D.L., Bleeker, W., Downs, R.T., Farquhar, J., Ferry, J.M., Grew, E.S., Knoll, A.H., Papineau, D., Ralph, J.P., Sverjensky, D.A., Valley, J.W., 2011. Needs and opportunities in mineral evolution research. Am. Mineral. 96, 953–963.
Hazen, R.M., Downs, R.T., Eleish, A., Fox, P., Gagné, O.C., Golden, J.J., Grew, E.S., Hummer, D.R., Hystad, G., Krivovichev, S.V., Li, C., Liu, C., Ma, X., Morrison, S.M., Pan, F., Pires, A.J., Prabhu, A., Ralph, J., Runyon, S.E., Zhong, H., 2019. Data-Driven Discovery in Mineralogy: Recent Advances in Data Resources, Analysis, and Visualization. Engineering 5, 397–405.
Hofmann, B.A., Knill, M.D., 1996. Geochemistry and genesis of the Lengenbach Pb-Zn-As-Tl-Ba-mineralisation, Binn Valley. Switzerland. *Miner. Deposita* 31, 319–339.
Hummer, D.R., Golden, J.J., Hystad, G., Downs, R.T., Eleish, A., Liu, C., Ralph, J., Morrison, S.M., Meyer, M.B., Hazen, R.M., 2022. Evidence for the oxidation of Earth's crust from the evolution of manganese minerals. Nat. Commun. 13, 960.
Hurtgen, M.T., Arthur, M.A., Halverson, G.P., 2005. Neoproterozoic sulfur isotopes, the evolution of microbial sulfur species, and the burial efficiency of sulfide as sedimentary pyrite. Geology 33, 41–44.
Ivanov M. V. (1983) Major fluxes of the global biogeochemical cycle of sulfur. In *The Global Biogeochemical Sulfur Cycle* John Wiley & Sons, Chichester, United Kingdom. pp. 449–463.
Jambor, J.I., Nordstrom, D.K., Alpers, C.N., 2000. Metal-sulfate salts from sulfide mineral oxidation. Rev. Mineral. Geochem. 40, 302–350.
Jelen, B.I., Giovannelli, D., Falkowski, P.G., 2016. The Role of Microbial Electron Transfer in the Coevolution of the Biosphere and Geosphere. Annu. Rev. Microbiol. 70, 45–62.
Johnson, J.E., Gerpheide, A., Lamb, M.P., Fischer, W.W., 2014. O2 constraints from Paleoproterozoic detrital pyrite and uraninite. GSA Bull. 126, 813–830.
Johnston, D.T., 2011. Multiple sulfur isotopes and the evolution of Earth's surface sulfur cycle. Earth Sci. Rev. 106, 161–183.
Jordan, S.F., Ioannou, I., Rammu, H., Halpern, A., Bogart, L.K., Ahn, M., Vasiliadou, R., Christodoulou, J., Maréchal, A., Lane, N., 2021. Spontaneous assembly of redox-active iron-sulfur clusters at low concentrations of cysteine. Nat. Commun. 12, 5925.
Konecke, B.A., Fiege, A., Simon, A.C., Parat, F., Stechern, A., 2017. Co-variability of S6+, S4+, and S2− in apatite as a function of oxidation state: Implications for a new oxybarometer. Am. Mineral. 102, 548–557.
Kress, V.C., Carmichael, I.S.E., 1991. The compressibility of silicate liquids containing Fe2O3 and the effect of composition, temperature, oxygen fugacity and pressure on their redox states. Contrib. Miner. Petrol. 108, 82–92.
Krivovichev, V.G., Krivovichev, S.V., Starova, G.L., 2023. Structural and Chemical Diversity and Complexity of Sulfur Minerals. Minerals 13, 1069.
Krouse, H.R., 1980. Sulphur isotopes in our environment. In: Handbook of Environmental Isotope Geochemistry I. The terrestrial environment. Elsevier, Amsterdam, Netherlands, pp. 435–472.
Lafuente, B., Downs, R.T., Yang, H., Stone, N., 2015. The power of databases: the RRUFF project. In: Armbruster, T., Danisi, R.M. (Eds.), Highlights in Mineralogical Crystallography. W. De Gruyter, Berlin, Germany, pp. 1–30.
Leavitt, W.D., Halevy, I., Bradley, A.S., Johnston, D.T., 2013. Influence of sulfate reduction rates on the Phanerozoic sulfur isotope record. Proc. Natl. Acad. Sci. 110, 11244–11249.
Liang, X., Kwok, C.Y., Lodi-Marzano, F., Pang, Q., Cuisinier, M., Huang, H., Hart, C.J., Houtarde, D., Kaup, K., Sommer, H., Brezesinski, T., Janek, J., Nazar, L.F., 2016. Tuning Transition Metal Oxide-Sulfur Interactions for Long Life Lithium Sulfur Batteries: The "Goldilocks" Principle. Adv. Energy Mater. 6, 1501636.
Liu, C., Runyon, S.E., Knoll, A.H., Hazen, R.M., 2019. The same and not the same: Ore geology, mineralogy and geochemistry of Rodinia assembly versus other supercontinents. Earth Sci. Rev. 196, 102860.
Lundy, W.T., 1950. Known and Potential Sulfur Resources of the World. Ind. Eng. Chem. 42, 2199–2201.
Luo, G., Ono, S., Beukes, N.J., Wang, D.T., Xie, S., Summons, R.E., 2016. Rapid oxygenation of Earth's atmosphere 2.33 billion years ago. Sci. Adv. 2, e1600134.

Makovicky, E., 2019. Algorithms for calculations of homologue order N in the homologous series of sulfosalts. Eur. J. Mineral. 31, 83–97.
Malyshev, A., Malysheva, L., 2022. Sulfur in ore formation. Ore Geol. Rev. 150, 105199.
Mateos, K., Chappell, G., Klos, A., Le, B., Boden, J., Stüeken, E., Anderson, R., 2023. The evolution and spread of sulfur cycling enzymes reflect the redox state of the early Earth. Sci. Adv. 9, eade4847.
McCammon, C., 2005. The Paradox of Mantle Redox. Science 308, 807–808.
McCammon, C., Kopylova, M.G., 2004. A redox profile of the Slave mantle and oxygen fugacity control in the cratonic mantle. Contrib. Miner. Petrol. 148, 55–68.
McDonough, W.F., Sun, S.S., 1995. The composition of the Earth. Chem. Geol. 120, 223–253.
McLoughlin, N., Grosch, E.G., Kilburn, M.R., Wacey, D., 2012. Sulfur isotope evidence for a Paleoarchean subseafloor biosphere, Barberton, South Africa. Geology 40, 1031–1034.
Moëlo, Y., Makovicky, E., Mozgova, N.N., Jambor, J.L., Cook, N., Pring, A., Paar, W., Nickel, E.H., Graeser, S., Karup-Møller, S., Balic-Žunic, T., Mumme, W.G., Vurro, F., Topa, D., Bindi, L., Bente, K., Shimizu, M., 2008. Sulfosalt systematics: a review. Report of the sulfosalt sub-committee of the IMA Commission on Ore Mineralogy. Eur. J. Mineral. 20, 7–46.
Moore, E.K., Jelen, B.I., Giovannelli, D., Raanan, H., Falkowski, P.G., 2017. Metal availability and the expanding network of microbial metabolisms in the Archaean eon. Nat. Geosci. 10, 629–636.
Moore, E.K., Hao, J., Prabhu, A., Zhong, H., Jelen, B.I., Meyer, M., Hazen, R.M., Falkowski, P.G., 2018. Geological and Chemical Factors that Impacted the Biological Utilization of Cobalt in the Archean Eon. J. Geophys. Res. Biogeosciences 123, 743–759.
Moore, E.K., Hao, J., Spielman, S.J., Yee, N., 2020. The evolving redox chemistry and bioavailability of vanadium in deep time. Geobiology 18, 127–138.
Moore, E.K., Golden, J.J., Morrison, S.M., Hao, J., Spielman, S.J., 2022a. The expanding network of mineral chemistry throughout earth history reveals global shifts in crustal chemistry during the Proterozoic. Sci. Rep. 12, 4956.
Moore, E.K., Martinez, D.L., Srivastava, N., Morrison, S.M., Spielman, S.J., 2022b. Mineral Element Insiders and Outliers Play Crucial Roles in Biological Evolution. Life 12, 951.
Moore, E.K., Ostroverkhova, A., Hummer, D., Morrison, S., Peralta, Y., Spielman, S.J., 2023. The influence of oxygen and electronegativity on iron mineral chemistry throughout Earth's history. Precambr. Res. 386, 106960.
Morrison, S.M., Runyon, S.E., Hazen, R.M., 2018. The Paleomineralogy of the Hadean Eon Revisited. Life 8, 64.
Morrison, S.M., Buongiorno, J., Downs, R.T., Eleish, A., Fox, P., Giovannelli, D., Golden, J.J., Hummer, D.R., Hystad, G., Kellogg, L.H., Kreylos, O., Krivovichev, S.V., Liu, C., Merdith, A., Prabhu, A., Ralph, J., Runyon, S.E., Zahirovic, S., Hazen, R.M., 2020. Exploring Carbon Mineral Systems: Recent Advances in C Mineral Evolution, Mineral Ecology, and Network Analysis. Front. Earth Sci. 8, 208.
Naldrett, A.J., Craig, J.R., Kullerud, G., 1967. The central portion of the Fe-Ni-S system and its bearing on pentlandite exsolution in iron-nickel sulfide ores. Econ. Geol. 62, 826–847.
Nordstrom, D.K., 1982. Aqueous Pyrite Oxidation and the Consequent Formation of Secondary Iron Minerals. In Acid Sulfate Weathering John Wiley & Sons, Ltd., pp. 37–56
Nowacki, W., Bürki, H., Iitaka, Y., Kunz, V., 1961. Structural investigations on sulfosalts from the Lengenbach, Binn Valley (Ct. Wallis). Part 2. Swiss Bull. Mineral. Petrol. 41, 103–116.
Parat, F., Holtz, F., Streck, M.J., 2011. Sulfur-bearing Magmatic Accessory Minerals. Rev. Mineral. Geochem. 73, 285–314.
Paszkowicz, W., Leiro, J.A., 2005. Rietveld refinement study of pyrite crystals. J. Alloy. Compd. 401, 289–295.
Pauling, L., 1932. The Nature of the Chemical Bond. IV. The energy of single bonds and the relative electronegativity of atoms. J. Am. Chem. Soc. 54, 3570–3582.
Peters, B., 1959. Cosmic-ray produced radioactive isotopes as tracers for studying large-scale atmospheric circulation. J. Atmospheric Terr. Phys. 13, 351–370.
Philippot, P., Zuilen, M.V., Lepot, K., Thomazo, C., Farquhar, J., Kranendonk, M.J.V., 2007. Early Archaean Microorganisms Preferred Elemental Sulfur, Not Sulfate. Science 317, 1534–1537.
Piccoli, P.M., Candela, P.A., 2002. Apatite in Igneous Systems. Rev. Mineral. Geochem. 48, 255–292.
R Core Team, 2021. R: A language and environment for statistical computing. R Foundation for Statistical Computing, Vienna, Austria.
Rakovan, J., 2007. Words to the Wise— More than 4,000 To Be Exact. Rocks Miner. 82, 423–424.
Raven, M.R., Fike, D.A., Bradley, A.S., Gomes, M.L., Owens, J.D., Webb, S.A., 2019. Paired organic matter and pyrite δ34S records reveal mechanisms of carbon, sulfur, and iron cycle disruption during Ocean Anoxic Event 2. Earth Planet. Sci. Lett. 512, 27–38.
Raven, M.R., Keil, R.G., Webb, S.M., 2021a. Microbial sulfate reduction and organic sulfur formation in sinking marine particles. Science 371, 178–181.
Raven, M.R., Keil, R.G., Webb, S.M., 2021b. Rapid, Concurrent Formation of Organic Sulfur and Iron Sulfides During Experimental Sulfurization of Sinking Marine Particles. Glob. Biogeochem. Cycles 35 e2021GB007062.
Raven, M.R., Crockford, P.W., Hodgskiss, M.S.W., Lyons, T.W., Tino, C.J., Webb, S.M., 2023. Organic matter sulfurization and organic carbon burial in the Mesoproterozoic. Geochim. Cosmochim. Acta 347, 102–115.
Rudnick R. L. and Gao S. (2003) 3.01 - Composition of the Continental Crust. In *Treatise on Geochemistry* (eds. H. D. Holland and K. K. Turekian). Pergamon, Oxford, U.K. pp. 1–64.
Sadove, G., Konecke, B.A., Fiege, A., Simon, A.C., 2019. Structurally bound S2−, S1−, S4+, S6+ in terrestrial apatite: The redox evolution of hydrothermal fluids at the Phillips mine, New York, USA. Ore Geol. Rev. 107, 1084–1096.
Sahoo, S.K., Planavsky, N.J., Kendall, B., Wang, X., Shi, X., Scott, C., Anbar, A.D., Lyons, T.W., Jiang, G., 2012. Ocean oxygenation in the wake of the Marinoan glaciation. Nature 489, 546–549.
Santosh, M., Groves, D.I., 2022. Global metallogeny in relation to secular evolution of the Earth and supercontinent cycles. Gondw. Res. 107, 395–422.
Sato, M., 1960. Oxidation of sulfide ore bodies. II. Oxidation mechanisms of sulfide minerals at 25 C. Econ. Geol. Bull. Soc. Econ. Geol. US Vol: 55.
Schröder, S., Bekker, A., Beukes, N.J., Strauss, H., Van Niekerk, H.S., 2008. Rise in seawater sulphate concentration associated with the Paleoproterozoic positive carbon isotope excursion: evidence from sulphate evaporites in the ~2.2–2.1 Gyr shallow-marine Lucknow Formation. South Africa. *Terra Nova* 20, 108–117.
Scott, S.D., Barnes, H.L., 1972. Sphalerite-wurtzite equilibria and stoichiometry. Geochim. Cosmochim. Acta 36, 1275–1295.
Scott, C., Lyons, T.W., Bekker, A., Shen, Y., Poulton, S.W., Chu, X., Anbar, A.D., 2008. Tracing the stepwise oxygenation of the Proterozoic ocean. Nature 452, 456–459.
Seal, R.R.I.I., 2006. Sulfur Isotope Geochemistry of Sulfide Minerals. Rev. Mineral. Geochem. 61, 633–677.
Seal, R.R.I.I., Alpers, C.N., Rye, R.O., 2000. Stable Isotope Systematics of Sulfate Minerals. Rev. Mineral. Geochem. 40, 541–602.
Shaw, G.H., 2008. Earth's atmosphere – Hadean to early Proterozoic. Geochemistry 68, 235–264.
Shen, Y., Buick, R., 2004. The antiquity of microbial sulfate reduction. Earth Sci. Rev. 64, 243–272.
Shen, Y., Buick, R., Canfield, D.E., 2001. Isotopic evidence for microbial sulphate reduction in the early Archaean era. Nature 410, 77–81.
Shen, Y., Farquhar, J., Masterson, A., Kaufman, A.J., Buick, R., 2009. Evaluating the role of microbial sulfate reduction in the early Archean using quadruple isotope systematics. Earth Planet. Sci. Lett. 279, 383–391.
Simon, A.C., Ripley, E.M., 2011. The Role of Magmatic Sulfur in the Formation of Ore Deposits. Rev. Mineral. Geochem. 73, 513–578.
Sinninghe Damste J. S. and De Leeuw J. W. (1990) Analysis, structure and geochemical significance of organically-bound sulphur in the geosphere: State of the art and future research. *Org. Geochem.* **16**, 1077–1101.
Spielman, S.J., Moore, E.K., 2020. dragon: A New Tool for Exploring Redox Evolution Preserved in the Mineral Record. Front. Earth Sci. 8.
Srivastava, N., Spielman, S.J., Morrison, S.M., Moore, E.K., 2021. Geological Factors Impacted Cadmium Availability and use as an Alternative Cofactor for Zinc in the Carbon Fixation Pathways of Marine Diatoms. J. Geophys. Res. Biogeosci. 126 e2020JG005966.
Strauss, H., 1999. Geological evolution from isotope proxy signals — sulfur. Chem. Geol. 161, 89–101.
Taylor, S.R., McLennan, S.M., 1995. The geochemical evolution of the continental crust. Rev. Geophys. 33, 241–265.
Temple, K.L., 1964. Syngenesis of sulfide ores; an evaluation of biochemical aspects. Econ. Geol. 59, 1473–1491.
Temple, K.L., Le Roux, N.W., 1964. Syngenesis of sulfide ores; desorption of adsorbed metal ions and their precipitation as sulfides. Econ. Geol. 59, 647–655.
Trail, D., Watson, E.B., Tailby, N.D., 2011. The oxidation state of Hadean magmas and implications for early Earth's atmosphere. Nature 480, 79–82.
Ueno, Y., Ono, S., Rumble, D., Maruyama, S., 2008. Quadruple sulfur isotope analysis of ca. 3.5Ga Dresser Formation: New evidence for microbial sulfate reduction in the early Archean. Geochim. Cosmochim. Acta 72, 5675–5691.
Vahrenkamp, H., 1975. Sulfur Atoms as Ligands in Metal Complexes. Angew. Chem. Int. Ed. Engl. 14, 322–329.
Vaughan, D.J., 2006. Sulfide Mineralogy and Geochemistry: Introduction and Overview. Rev. Mineral. Geochem. 61, 1–5.
Veizer J. and Mackenzie F. T. (2014) The Evolution of Sedimentary Rocks. In *Treatise on Geochemistry* pp. 399–435.
Voice, P.J., Kowalewski, M., Eriksson, K.A., 2011. Quantifying the Timing and Rate of Crustal Evolution: Global Compilation of Radiometrically Dated Detrital Zircon Grains. J. Geol. 119, 109–126.
Wasserman, S., Faust, K., 1994. Social Network Analysis: Methods and Applications. Cambridge University Press.
Werne J. P., Hollander D. J., Lyons T. W. and Sinninghe Damsté J. S. (2004) Organic sulfur biogeochemistry: Recent advances and future research directions. In *Sulfur Biogeochemistry - Past and Present* (eds. J. P. Amend, K. J. Edwards, and T. W. Lyons). Geological Society of America. p. 0.
Westall F., Ronde C. E. J. de, Southam G., Grassineau N., Colas M., Cockell C. and Lammer H. (2006) Implications of a 3.472–3.333 Gyr-old subaerial microbial mat from the Barberton greenstone belt, South Africa for the UV environmental conditions on the early Earth. *Philos. Trans. R. Soc. Lond. B Biol. Sci.* **361**, 1857–1876.
Whitney, J.A., Jr, S.J.C., 1983. Igneous sulfides in the Fish Canyon Tuff and the role of sulfur in calc-alkaline magmas. Geology 11, 99–102.
Williams, R.J.P., 1981. The Bakerian Lecture, 1981 Natural Selection of the Chemical elements. Proc. R. Soc. Lond. B 213, 361–397.
Williams, E.G., Keith, M.L., 1963. Relationship between sulfur in coals and the occurrence of marine roof beds. Econ. Geol. 58, 720–729.
Windley, B.F., Kusky, T., Polat, A., 2021. Onset of plate tectonics by the Eoarchean. Precambr. Res. 352, 105980.

Wood, B.J., Virgo, D., 1989. Upper mantle oxidation state: Ferric iron contents of lherzolite spinels by 57Fe Mössbauer spectroscopy and resultant oxygen fugacities. Geochim. Cosmochim. Acta 53, 1277–1291.
Xu, T., Pruess, K., 2001. On fluid flow and mineral alteration in fractured caprock of magmatic hydrothermal systems. J. Geophys. Res. Solid Earth 106, 2121–2138.
Ye, L., Cook, N.J., Ciobanu, C.L., Yuping, L., Qian, Z., Tiegeng, L., Wei, G., Yulong, Y., Danyushevskiy, L., 2011. Trace and minor elements in sphalerite from base metal deposits in South China: A LA-ICPMS study. Ore Geol. Rev. 39, 188–217.